J Therm Anal Calorim (2014) 117:557–566
DOI 10.1007/s10973-014-3775-6

Thermo-physical characterization of some paraffins used as phase change materials for thermal energy storage

E. M. Anghel · A. Georgiev · S. Petrescu · R. Popov · M. Constantinescu

Received: 30 September 2013 / Accepted: 17 March 2014 / Published online: 12 April 2014

Abstract Three phase change paraffinic materials (PCMs) were thermophysically (phase-transition temperatures, latent heat, heat capacity at constant pressure, density, and thermal conductivity) investigated in order to be used as latent heat storage media in a pilot plant developed in Plovdiv Bulgaria. Raman structural investigation probes aliphatic character of the E53 sample, while the E46 and ECP samples contain also unsaturated components due to their Raman features within 1,500–1,700 cm^{-1} range. Orthorhombic structure of the three PCMs was evidenced by the Raman modes at the 1,417 cm^{-1}. The highest latent heat value, ΔH, of phase transitions among the three materials was represented by summation of a solid order–disorder, and melting latent heat was encountered by the E53 paraffin, i.e., 194.32 J g^{-1} during a μ-DSC scan of 1 °C min^{-1}. Conversely, the ECP composite containing ceresin component shows the lowest latent heat value of 143.89 J g^{-1} and the highest thermal conductivity of 0.46 W m^{-1} K^{-1} among the three phase change materials (PCMs). More facile melt-disordered solid transition with the activation energy of 525.45 kJ mol^{-1} than the lower temperature transition of disorder–order (E_a of 631.73 kJ mol^{-1}) during the two-step process of solidification for the E53 melt are discussed in terms of structural and molecular motion changes.

Keywords Latent heat storage · Phase change material · Raman spectroscopy · DSC · Paraffin · Composite

E. M. Anghel (✉) · S. Petrescu · M. Constantinescu
Romanian Academy, Institute of Physical Chemistry ''Ilie Murgulescu'', Spl. Independentei 202, 060021 Bucharest, Romania
e-mail: eanghel@hotmail.com

A. Georgiev
Department of Mechanics, Technical University of Sofia, Branch Plovdiv, Plovdiv, Bulgaria

R. Popov
Department of Optoelectronics and Laser Engineering, Technical University of Sofia, Branch Plovdiv, Plovdiv, Bulgaria

Introduction

The application of the phase change materials (PCMs) in thermal energy storage has been well known in many fields, such as in solar energy storage [1], waste heat recovery [2], and smart air conditioning in buildings [3]. Prior selection of the PCMs for heating and cooling purposes in buildings, several criteria [4] concerning PCM's thermophysical properties (suitable phase-transition temperature, high latent heat of transition, good heat transfer, high density, small volume change, and thermal stability), kinetic properties (high crystallization rate, no supercooling), chemical properties (reversible melt/freeze cycles, non-flammable, non-toxic, capability with other building materials), economic (abundance and low prices), and environment issues (non-polluting, recycling potential) should be considered. A comprehensive knowledge of thermal stability of the PCMs as functions of number of repeated thermal cycles is essential to ensure the long-term performance and economic feasibility of the latent heat storage systems [5]. Therefore, considerable research efforts have been dedicated improving the existing PCMs [5–8] and identifying new materials with desirable thermal properties [9, 10].

Among the organic PCMs, paraffins were extensively studied for latent heat storage purposes due to their large latent heat of melting (moderate thermal storage densities of ~200 kJ kg^{-1} or 150 MJ m^{-3}) [11], good stability,

negligible subcooling, as well lack of toxicity and low prices [1, 2, 5–8]. However, low thermal conductivity (bellow 0.4 W $m^{-1}K^{-1}$), large volume change, leaking, and high flammability hamper integration of paraffins into latent heat storage systems. To overcome the low thermal conductivity and implicitly decrease of their thermal resistance to the heat transfer, graphite [12] as well as other conductors such as aluminum, nickel, cooper [8, 13], or some composites have been added. Besides, metal foams from the paraffin-containing composites ensure low bulk density due to its high open porosity, high specific strength and stiffness, and especially high thermal conductivity for continuous skeleton structure [8, 13].

Commercial paraffin waxes, i.e., C_nH_{2n+2} hydrocarbons, are chain polymers which crystallize in lamellar form [14, 15]. The level of crystallinity achieved by these polymers has a major effect on its thermal properties such as dimensional stability and high temperature performance. Also, thickness of the crystalline lamellae depends on its processing parameters (thermal histories, cooling rates) and polymer chemistry (molecular length, polymer chain make-up, nucleating agents, molecular mass distribution, etc.) [14, 15].

Early stages in developing and/or optimizing of the heat storage systems consist in accurate measurement of the thermo-physical data of the PCMs. However, inconsistent data [16–18] were supplied by various groups of authors due to limitations of the conventional thermal analysis methods such as differential scanning calorimetry DSC, i.e., dependence of the thermal response on the heating/cooling rate, sample mass (typically less than 90 mg), and apparatus calibration. Phase change temperature, latent heat, and heat capacity are few thermophysical data supplied by broadly used DSC [18]. Since the sample mass and the heating/cooling rate are sensible parameters in DSC techniques, small heating rate was recommended for the small mass in order to avoid measuring errors [19]. First DSC investigations of the paraffin waxes were carried about in connection with the small wax content of the crude oil as well as in the distillated fuels which can cause damages of the industrial equipments and engines in cold climate [18]. X-ray diffraction (XRD), IR, and NMR spectroscopy were the most employed techniques for structural characterization of the paraffin waxes.

The aim of this work was to thermophysically characterize (phase change temperature, latent heat, heat capacity, density, and volume variation) the two commercial paraffin waxes, named E53 and E46, and a commercial paraffin-ceresine composite (ECP) in order to implement them in a heat storage pilot plant developed in Plovdiv, Bulgaria [20, 21]. Fitting of the PCM crystallization exotherms of the DSC curves is attained by using spectroscopic and chromatography element as described, elsewhere [22], in accordance to the structural information here obtained from Raman spectroscopy.

Experimental

Materials

Two commercial-grade paraffins: E53 (0.8–1 % oil content) and E46 (0.7–1.5 oil content) and a commercial paraffinic composite with ceresine (3–6 % oil content), ECP, from Evricom Ltd, Bulgaria were tested as PCMs (% stands for mass percentage). The ceresine component, a microcrystalline wax derived from ozokerite, also enables shape stabilization and electric insulation of the resulted composite.

Methods for thermo-physical characterization

μ-DSC measurements

These measurements were carried out in a SETARAM Micro DSC VII Evo with an outer thermostatic loop provided by a Julabo F32-HE device operating in standard mode. The 3D sensor protection was purged with Nitrogen purge gas (99.99 % SIAD -TP). Samples of 9–11 mg of the paraffin samples were placed in standard Hastelloy cells with an empty cell for reference. The measurement procedure was started with a set of calibration measurements. Each calibration was performed on standard materials and was used to determine the sensitivity at one temperature, which is the melting temperature of that standard material [14]. The heat flow measurements were recorded with a rate of 1 °C min^{-1}, during two cycles to check the thermal history and hence to probe the thermal reproducibility. Calisto V 1.051 software was used for data acquisition and primary signal processing. The resulted split and asymmetrical DSC curves were analyzed and processed in Peak Fit software, and the multi-component decomposition was used for DSC curves. Multiple-component fitting of the melting/freezing (charge/discharge) peaks is based on the macromolecular chain modifications of the PCMs, the n-folded chains where $n = 0$, 1, and 2, existing simultaneously in the PCM polymers with low molar masses [22].

For specific heat capacity, C_p data, empty cell and sapphire were utilized as blank and reference respectively in DSC measurements. The C_p values were also determined with Calisto software.

DSC measurements

To obtain the heating/cooling rate influence on the thermal data and the glass transition, T_g, of the E53 paraffin, a

Perkin Elmer DSC 8500, operating within −180 to 750 °C temperature range, under a nitrogen flow of 20 mL min^{-1} was used. Temperature and melting enthalpy were calibrated with standard indium. The thermal history of the samples was erased by heated up at 70 °C with a 16 °C min^{-1} rate, hold for 10 min, and cooled down with the same rate up to −70 °C. T_g value was measured on the second cycle on heating. Also, heat flow during solidification of small samples, about 2 mg, at higher DSC scanning rates of 1, 5, 8 10, and 16 °C min^{-1} were carried out for further non-isothermal kinetic computing (simple Kissinger approach [23]). Baseline correction and peak integration of the DSC signals were performed by the Pyris™ software.

Thermal conductivity and effusivity

Small cylinders of paraffinic samples (1.8 × 1=d × h) were tested for thermal conductivity and effusivity by means of a C-Therm TCi Analyzer, at room temperature. The Thermal Analyzer was calibrated against the Pyrex reference. Water was employed as contact agent. The thermal effusivity, e, describes the ability of a material to exchange heat with its surroundings. It is presented with the following equation:

$$e = \sqrt{\lambda.\rho.c_p} \quad (1)$$

Density measurements and volume variation

The determining density of solid–liquid used two different methods: for solid samples, the Pycnometer (25 cm^3) method was used, while a hydrostatic balance densimeter with a platinum (Pt) sinker was employed for molten samples. Density of small specimens ranging from 220 to 260 mg of the PCMs was measured by weighing in air and dividing this mass by the buoyancy when the sample is sink in water heated up to 30 °C. As for the molten PCMs, mass of the Pt sphere connected by a Pt wire to the weighing hook of a commercial analytical balance and immersed in the paraffinic melt is measured as a function of temperature of the melt, T, [24]:

$$\rho_T = \frac{m - m_T^*}{V_T} \quad (2)$$

where m and m_T^* are the "true" mass of the sinker and apparent mass of the liquid displaced by the sinker, and V_T is the sinker volume at different temperatures. Volume change during the phase transition is an important parameter for dimensioning the heat storage systems. This variation was determined from density data.

Raman spectroscopy

Unpolarized solid state Raman spectra were recorded by means of a LabRam HR spectrometer (Jobin–Yvon–Horiba) over 50−3,600 cm^{-1} range. The 514 nm line of an Ar^+ laser was used as an exciting radiation through a 50× objective of an Olympus microscope in a backscattering geometry and at a confocal hole of 200 µm. The scanning parameter for each Raman spectrum taken as 5 s and 10 scans was accumulated. The diameter of the laser spot on the sample surface amounted to about 1 µm providing a spectral resolution better than 2 cm^{-1}. The polynomial correction of the fluorescent background for the ECP and E46 samples was performed by means of the Origin software. Moreover, Raman spectrum of the E53 paraffin was recorded after its thermal history was erased by heating a small sample (2 mg) up to the 70 °C for 10 min., cooled down to the −70 °C followed by heating up at room temperature as described earlier in 2.2.2. Longer accumulations, 10 s and 20 scans, enabled obtaining acceptable E53 spectrum within 800–1,700 and 2,600–3,100 cm^{-1} domains.

Results and discussions

The development of the PCM containing systems involves understanding of the heat transfer in PCMs when they undergo solid–liquid phase transition in the required operating temperature range. The study of the phase change behavior, absorption, and evolving of heat emphasizes the dependence of this process on both internal structure of the polymer and the applied treatment: cooling/heating velocity, thermal history. An analysis of morphological and structural characterization of PCMs, their physico-chemical stability as well as thermo-physical properties was

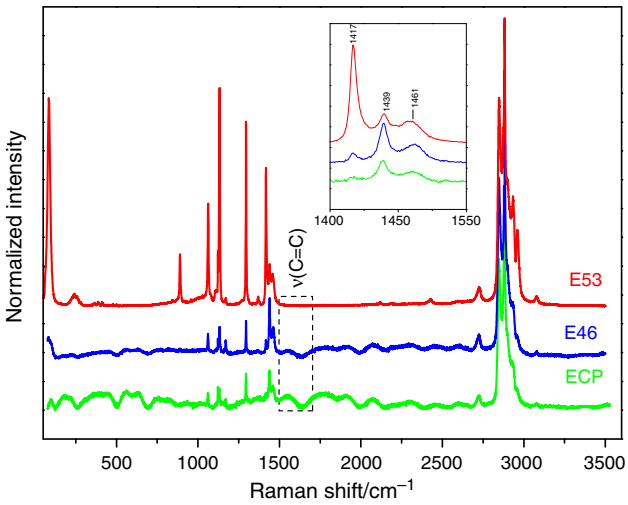

Fig. 1 Raman spectra of the E46, ECP samples (fluorescent background corrected), and E53 sample (50 s acquisition time). *Inset* represents the methylene bending frequencies of the E53, E46, and ECP samples within 1,400–1,500 cm^{-1} range

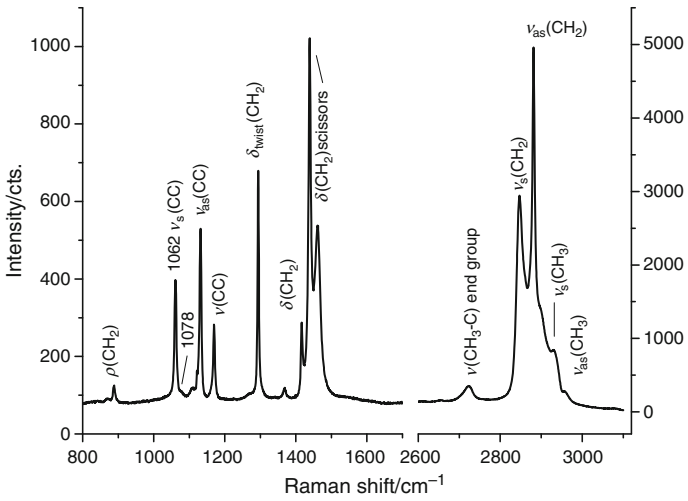

Fig. 2 Raman spectrum of the thermally erased history of E53 paraffin (200 s acquisition time) at room temperature. Assignments were made according to references [25–27]

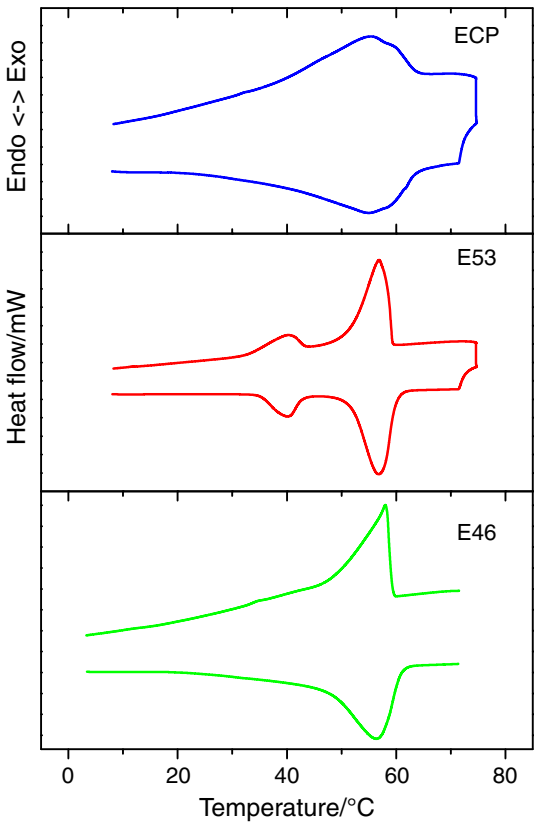

Fig. 3 DSC runs for the E53, E46, and ECP samples recoded with a 1 °C min^{-1} rate (μ-DSC SETARAM)

performed by using characterization equipment and methods able to test materials from nano-scale to macro-scale.

Raman spectra

Raman spectra of the three PCMs are illustrated in Fig. 1. Slightly wider spectral features of the E46 and ECP samples indicate more pronounced amorphous character of the two samples. Lack of the spectral features within 1,500–1,700 cm^{-1} assignable to the stretching of the C=C bondings [25, 26] in the Raman spectrum of the E53 paraffin probes its saturate character contrary to the other two samples ECP and E46. The ceresine (a mixture of unsaturated and branched hydrocarbons obtained from ozokerite [27]) content of the ECP sample gave its unsaturated character (the most intense spectral features within 1,500–1,700 cm^{-1} range in comparison to the E46 sample).

Table 1 Thermal data (latent heat, ΔH, phase change temperatures) of the E46, ECP, and E53 samples from the μ-DSC runs at 1 °C min^{-1} rate

Sample	Cycle	T_{on}/°C	T_{max}/°C	T_{off}/°C	ΔH/J g^{-1}
E53[a]	Heating	33.07	39.83	45.33	194.32
		51.79	56.4	59.22	
	Cooling	59.41	57.01	51.93	−194.11
		44.36	39.76	33.02	
E46	Heating	46.67	56.57	61.78	176.77
	Cooling	59.54	56.99	47	−165.69
ECP	Heating	43.85	54.21	64.00	143.891
	Cooling	63.39	55.51	34.03	−142.9

[a] DSC signal fitting with an exponentially modified gaussian (EMG) band profile

Comparing the Raman spectra of the E53 paraffin in Fig. 1 and Fig. 2 (raw and with thermally history erased), no new bands but intensity band variations were recorded. The high frequency Raman domain over 2,600–3,100 cm^{-1}, assignable to the C–H stretching, was used to monitor phase transition in paraffin waxes [26]. This domain in Fig. 2 for the E53 spectrum is dominated by the stretching vibrations (2,849 and 2,883 cm^{-1}) of the methylene groups (CH_2) in the paraffin chains. Presence of the methyl (CH_3) groups is marked by two shoulders at 2,932 and 2,958 cm^{-1} of the latter strong band peaking up at 2,883 cm^{-1}.

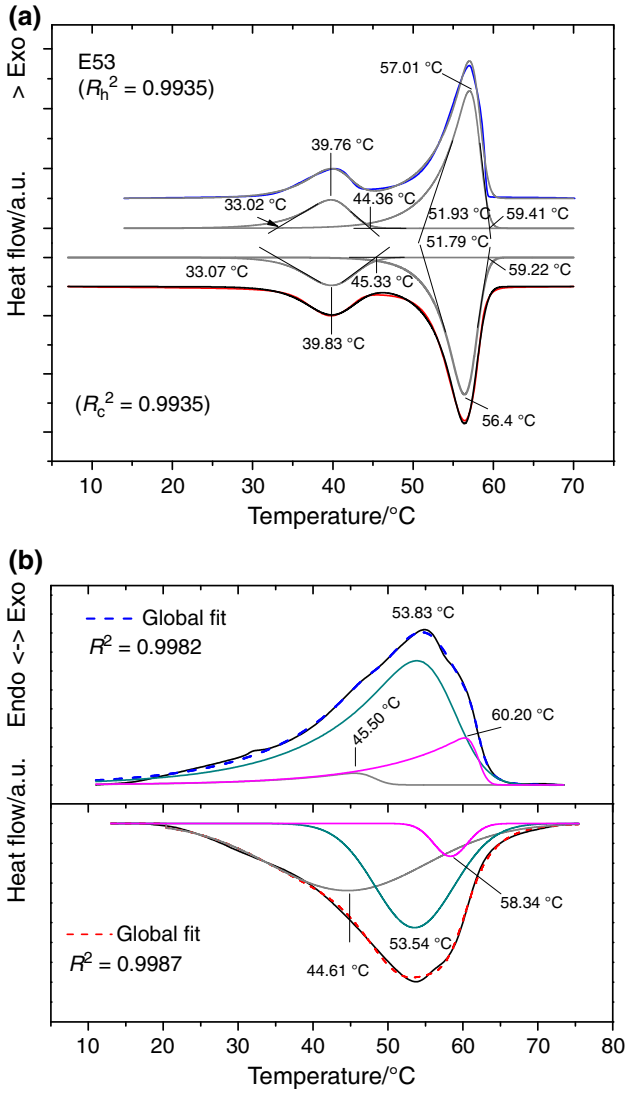

Fig. 4 EMG fitting of the μ-DSC curves on heating/cooling for: **a** E53 and **b** ECP samples (DSC scanning rate of 1 °C min^{-1})

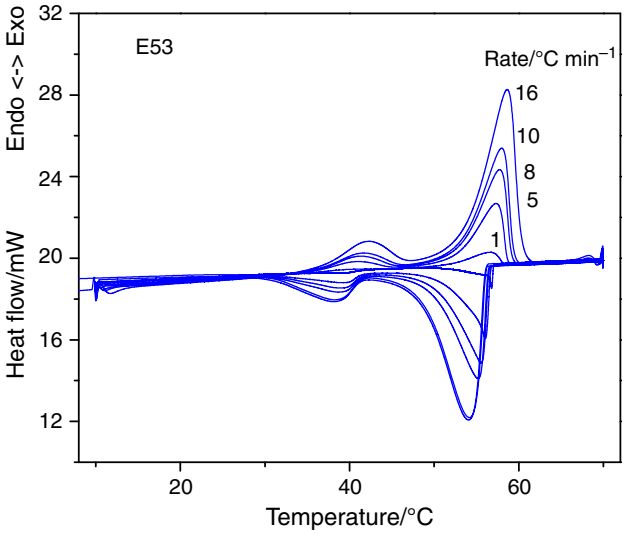

Fig. 5 Heating-cooling DSC cycles of the E53 (no thermal history) collected with 1, 5, 8, 10, and 16 °C min^{-1}

Stretching modes of the end-groups are signaled by the band at 2,723 cm^{-1}. The weak band at 3,077 cm^{-1} in all Raman spectra in Fig. 1 is assignable to the stretching C=C olefin mode very likely due to the oil content of the three PCMs. However, this band is missing in the Raman spectrum of the heat treated E53 in Fig. 2.

The two bands at 1,062 and 1,078 cm^{-1} in the 800–1,600 cm^{-1} domain (Fig. 2) were reported in the literature [26] as originating from two conformational states in paraffins namely *extended chain state* with consecutive all-trans bonds and *non-extended chain state*, respectively. Sharp bands at 1,062 and 1,132 cm^{-1}, corresponding to the frozen molecular motion to the location and to the hidden rotational modes [26], show that among closely packed extended chains interactions occur. Since the 1,078 cm^{-1} shoulder is relatively weak, the non-extended chain state in the E53 paraffin is relatively scarce. The same band at 1,062 cm^{-1} in Raman spectrum of the ECP with ceresine (Fig. 1) might have also *ν*(CO) assignment [27] due to aerial oxidation at unsaturated sites. The Raman bands in the 1,200–1,600 cm^{-1} region correspond to the bending in the methylene group [27]. The 1,420 cm^{-1} band (here at 1,417 cm^{-1} for the E53 paraffin in the inset of the Fig. 1) of the *n*-alkanes, considered to be crystal structure dependant [28], is also named crystallinity band. Thus, only orthorhombic and monoclinic unit cells with two molecules have this band. According to the odd and even number *n* (where *n* stands for number of the carbon atoms), the C_nH_{2n+2} can be orthorhombic (*n*-odd > 9) and triclinic (*n*-even > 6) [14, 29]. The more intense 1,417 cm^{-1} band for the E53 paraffin among the three PCMs points out its higher crystallinity. Crystal-field splitting of the methylene bending modes at about 1,440 cm^{-1} gave components separated by about 20 cm^{-1} [28]. Moreover, the triplet 1,417/1,439/1,461 cm^{-1} in Fig. 2 is markedly different than the one (1,417/1,439/1,459 cm^{-1}) in Fig. 1 for the same E53 sample bearing the thermal history information. As known [30], frequency modification of the triplet components triggers intensity modifications of the C–H asymmetric stretching modes in the high frequency of the Raman spectrum. Demising processes can take place in the alkanes with different chain lengths and hence different structures [31].

The two very weak bands at 850 and 869 cm^{-1} due to the molecular rotation for molten paraffins in the Raman spectrum of E53 (Fig. 2) might indicate presence of a small fraction of the liquid phase either due to an incomplete phase transition at room temperature or due to laser effect during spectrum recording.

Table 2 Dependence of thermal on heating/cooling rates data for the E53 paraffin

Rate/°C min^{-1}	Cycle	ΔH_1/Jg^{-1}	ΔH_2/Jg^{-1}	Peak 1			Peak 2			ΔH^a/J g^{-1}
				T_{on}/°C	T_{max}/°C	T_{off}/°C	T_{on}/°C	T_{max}/°C	T_{off}/°C	
16	Heating	26.61	136.54	36.1	42.09	46.24	53.59	58.65	60.28	198.50
	Cooling	−26.38	−131.89	41.22	38.13	30.94	55.96	54.14	48.51	−192.44
10	Heating	28.60	133.62	36.64	41.33	45.64	53.18	58.0	59.36	199.57
	Cooling	−27.37	−131.53	41.33	36.64	32.91	56.32	55.25	49.95	−193.76
8	Heating	28.57	133.89	36.16	41.21	44.96	53.0	57.76	59.11	200.54
	Cooling	−26.35	−128.32	41.39	39.04	34.72	56.45	55.55	50.62	−195.24
5	Heating	29.36	131.98	36.94	40.74	43.62	52.99	57.33	58.64	202.58
	Cooling	−28.02	−128.18	41.22	39.60	36.13	56.65	56.06	53.62	−194.30
1	Heating	38.0	148.46	27.14	39.64	41.22	50.79	56.69	58.06	224.64
	Cooling	−32.54	−126.27	42.95	39.82	31.6	56.99	56.77	56.44	−185.08

[a] Latent heat of the two peaks subsequent to the linear baseline correction

Due to the structural similarities between E46 and ECP samples, in the following discussions will focus mostly on the E53 paraffin and the ECP composite.

Thermal properties

The thermal data from the μ-DSC curves collected during the second heating/cooling cycle (Fig. 3) of the three PCMs under discussion are presented in Table 1. On the whole, the data agreement is satisfactory for the RAL standard (accuracy of the specific enthalpy within 10 % and of the temperature phase change of ±0.5 °C [19]). The latent heat of the melting process decreases in succession: E53 (194.32 J g^{-1}) > E46 (176.77 J g^{-1}) > ECP (143.89 J g^{-1}). The latent heat of the solidification process follows the same order. Contrary to the E46 and ECP samples with single asymmetric DSC peaks, the DSC curves on heating and cooling show two peaks (Figs. 3, 4a). Choosing an exponentially modified Gaussian (EMG) band profile for fitting the DSC signals is required by the highly asymmetric peaks in case of the E46 and ECP samples, not purely paraffin samples as pointed out earlier by Raman spectroscopy. According to the literature data [15], paraffins undergo multi-step phase transition, i.e., the lower temperature transitions are the solid–solid phase transitions, while the highest temperature transition represents the melting process. The order–disorder transitions represent the solid–solid phase transitions in paraffins [15, 18, 26]. Hence, the latent heat values included in the Table 1 are cumulative values of the solid–solid and solid–liquid phase transitions. Melting temperature of 56.4 °C (T_{on} of 51.8 °C in Table 1 and Fig. 4a) of the E53 point out its content of *n*-heptacosane $C_{27}H_{56}$ [32]. Three-peak fitting model was assumed for the DSC signal of the two samples E46 and ECP samples. The first two-phase transitions of the ECP represent the paraffin component (melting temperature of 53.7 °C corresponds to

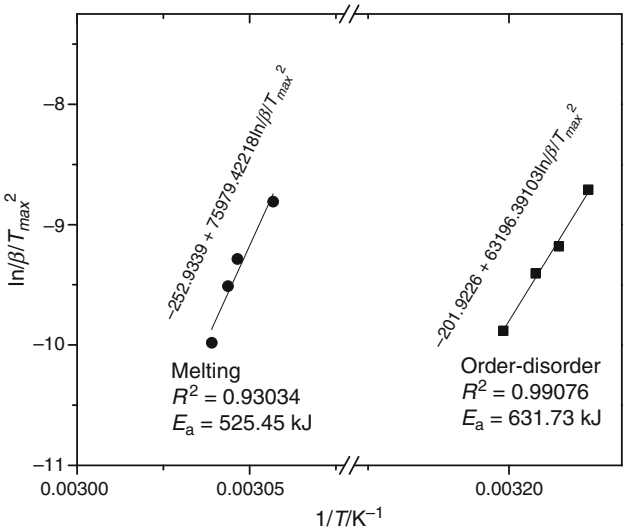

Fig. 6 Simple Kissinger plots of the E53 paraffin (no thermal history)

the *n*-pentacosane, $C_{25}H_{52}$ [32]), while the third peak at 58.34 °C on heating belongs to the ceresin component (Fig. 4b), typically with melting temperature within 54.4–90.6 °C range. Dirand et al. [29] showed that melting temperatures and transition enthalpies of the *n*-alkanes are highly dependant of the periodicity of the molecule layer packing along their axis and implicitly the carbon atom number. Thus, DSC derived melting points of the E53 paraffin and ECP composite support the Raman finding that these materials with orthorhombic structure have odd number carbon chains, i.e., 27 and 25, respectively. Knowledge of the type and numbers of the solid phases is important in dimensioning the latent heat storage in buildings [33]. Thus, a multi-solid front of solidification was forwarded by us in order to dimension a laboratory scale set-up containing a semicrystalline PCM, polyethylene glycol [33].

Table 3 C_p values of the E46, E53, and ECP samples recorded on a cooling cycle of 1°C min^{-1} rate

Sample	ΔT/°C	Regression Range/°C	Equation
E46	5 to 75	70.11–63.55	Liquid: 3.938554E+3−3.497555E+1·T+1.035792E−1·T^2−1.022529^{-4}·T^3
		16.21–8.63	Solid: 6.005763E+3−6.257255E+1·T+2.172568E−1·T^2−2.513133E−4·T^3
E53	5 to 70	67.06–61.52	Liquid: 1.099205E+5−9.730508E+2·T+2.870962E+0·T^2−2.823221E−3·T^3
		28.19–10.93	Solid: −1.141169E+3+1.166809E+1·T−3.975425E−2·T^2 + 4.520263E−5·T^3
ECP	−10 to 85	8.04–−6.17	Solid: −3.839858E + 2+4.306089E + 0·T−1.608291E−2·T^2 + 2.005564E−5·T^3
		80.28–70.20	Liquid 5.558095E+3−4.708851E + 1·T + 1.330327E−1·T^2−1.253053E−4·T^3

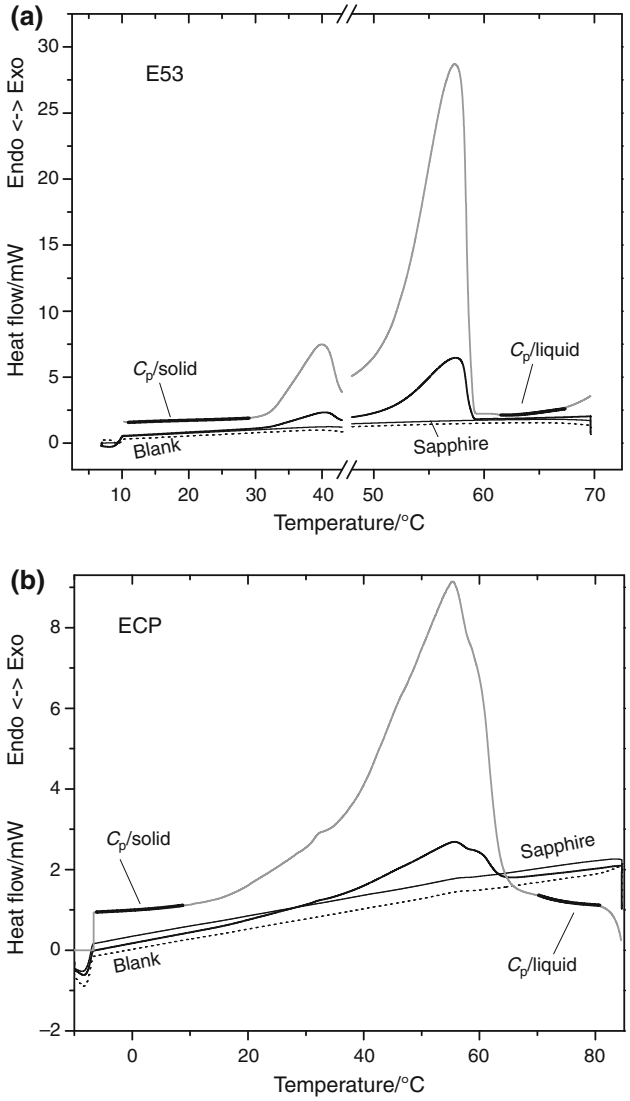

Fig. 7 Specific heat capacity (C_p) and its regression parameters for solid and liquid of the **a** E53 paraffin and **b** ECP composite obtained at cooling rate of 1°C min^{-1}

The thermal history and heating/cooling rates are two interdependent parameters that trigger suitable functionality of the storage material; therefore, they have to be monitored and with an appropriate modeling the system can be

Table 4 Effusivity, e, and thermal conductivity, $\boldsymbol{k}$, for the three PCMs: E46, E53, and ECP

Sample	e/ W m^{-2} k^{-1} s$^{1/2}$	$\boldsymbol{k}$/ W m^{-1} K^{-1}	$T_{ambient}$/ °C	ΔT/ °C	V_0/mV
E46	661	0.32	21.59	0.85	2,510.30
	667	0.32	22.57	0.85	2,509.02
	670	0.33	22.11	0.84	2,512.57
	670	0.33	22.05	0.84	2,512.97
	667	0.32	22.17	0.85	2,512.50
ECP	816	0.46	21.44	0.76	2,506.32
	814	0.45	21.62	0.76	2,507.42
	816	0.46	21.68	0.76	2,508.88
	818	0.46	21.99	0.76	2,508.64
	818	0.46	22.45	0.76	2,508.04
E53	688	0.34	23.02	0.82	2,510.47
	682	0.34	22.77	0.83	2,509.71
	679	0.33	22.76	0.83	2,509.97
	678	0.33	22.14	0.83	2,511.35
	679	0.33	22.73	0.83	2,509.74

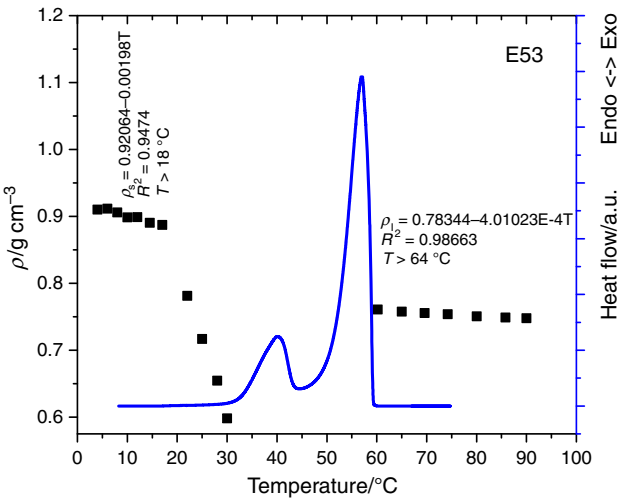

Fig. 8 Density and DSC heat flow of the E53 paraffin in solid and liquid phases (see Table 5)

Table 5 Density, ρ, and volume variation, ΔV_{PC}, of the three paraffinic PCMs

Sample	ΔT	Regression range/°C	Equation	ΔV^{a}_{PC}/%
E46	3 to 87	87–67	ρ (l) = 0.76728−7.08688E−5×T	12.4 %
		3–12	ρ (s) = 0.85759 + 4.00041E−5×T	
E-53	3 to 90	90–64	ρ (l) = 0.78344−4.01023E−4×T	16.3 %
		3–18	ρ (s) = 0.92064−0.00198 × T	
ECP	−3 to 97	97–77	ρ (l) = 0.94	20.3 % $T < 10$ °C
				12.5 % $T < 20$ °C
		5–10	ρ (s) = 0.7701−0.02174 × T	

[a] PC stands for phase change from ordered solid to liquid. L and s are the solid and liquid phases

dimensioned for a practical use. Hence, influence of heating/cooling rates and sample thermal history on the DSC data was tested by DSC runs at 1, 5, 8, 10, and 16 °C min^{-1} rates for the E53 paraffin. In Fig. 5, all endothermal peaks exhibit asymmetric left fronted shoulders with decreasing intensity toward slower rates as can be observed. A clear dependence of DSC curves on the heating/cooling rates, i.e., changes of the peak shapes, temperatures, and areas, was evidenced. A low cooling rate allows the formation of the thermodynamically more stable modifications. Thus, the stable extended chain ($n = 0$) has the lowest melting point among the n-folded chains. Thus, it is necessary to establish a suitable heating/cooling regime for application in order to evolve the maximum heat in a shorter time. Although μ-DSC data were collected during the second heating/cooling cycle (Table 1), different T_{on} and T_{off} values were recorded for the E53 with thermally history erased at the same 1 °C min^{-1} rate (Table 2). Moreover, the crystallinity of a polymer depends on its annealing treatment. For instance, in case of crystallization starting at temperatures close to the melting point, it is possible that some small regions from the polymer remain, and they play the role of preexistent nuclei for crystallization. The formed solid consists of building lamellae forming larger structures as spherulites [34]. In this case, many spherulites with small size will be observed. Also, the latent heat value of 224.64 J g^{-1} in Table 2 was calculated by integration of the two endothermal peaks for the E53 with no thermal history in comparing to the latent heat of 194 J g^{-1} (in Table 1) recorded during the second heating cycle of the raw E53. Both values were obtained after linear baseline correction. However, using a sigmoid baseline correction, the latent heat value obtained (Table 2) is 186.46 J g^{-1} (38 + 148.46 J g^{-1}), much closer to the one (194) J g^{-1} in Table 1. Despite the trivial importance granted to the baseline correction, the baseline of the DSC signal bears signature of the temperature dependence of the heat capacity for all reactants as well as products throughout a process [35], here the phase change processes.

The liquid–solid phase change occurs in a temperature interval where the two phases (liquid and solid) can coexist in equilibrium. During the process, when solidification starts at temperature T_{on} and ends at temperature T_{off}, between these two values an interphasic structure called "mushy zone" appears, where the preexistent nuclei are flowing in liquid [33].

The activation energy for melting/solidifying of the E53 with no thermal history was estimated by Kissinger equation [23]:

$$\ln\left(\frac{\beta}{T_{max}^2}\right) = \frac{E_a}{R}\left(\frac{1}{T_{max}}\right) + C \quad (3)$$

where β is the heating rate of 5, 8, 10, and 16 °C min^{-1}, R is the gas constant, T_{max} is the temperature of the maximum melting peak, and E_a is the apparent activation energy of the phase change for a PCM. In this case, the slope of the (β/T^2_{max}) versus $1/T_{max}$ plot, E_a/R) is used to obtain the E_a values for the two-phase transitions during solidification of the E53 melt, i.e., 525.45 kJ mol^{-1} for the solidification of the disordered solid, while ordering of the latter solid phase requires a higher E_a value of 631.73 kJ mol^{-1} (Fig. 6). More facile melt-solid transition than disordered solid-ordered solid transition can be discussed in terms of their structural and molecular motion changes. Thus, weakening of the molecular rotation and formation of the extended chain state on the expense of the non-extended chain state take place during melt solidification while further weakening of the molecular rotation, decreasing of the gauche defects and increasing of the fraction of longer, extended and closely packed chains causing enhancement of the paraffin crystallinity during disorder–order transition [26]. Presence of the packed extended chains in the ordered E53 solid was already identified by the two Raman bands at 1,062 and 1,132 cm^{-1}.

Additional thermo-physical data for heat storage modeling

Heat capacity of a PCM is an important physical parameter which provides information on additional sensible heat storage. Regression equations on the experimental data of the

specific heat capacity from the DSC curve, C_p, for solid and liquid, respectively, for all the studied materials are presented in Tables 3 and Fig. 7 for the E53 paraffin and ECP composite. Very low C_p values were calculated by regression for the three PCMs at 10 °C, namely 1.55 kJ kg^{-1} K^{-1} for E53 and E46, while ECP has the lowest C_p value of 1.14 kJ kg^{-1} K^{-1}. According to the T_{on} values for crystallization process (Table 1), the heat capacity of the molten E53 (at 60 °C), E46 (at 60 °C), and ECP (at 65 °C) is 2.36, 1.71 and 2.45 kJ kg^{-1} K^{-1}, respectively. These values are also thermal history and porosity dependent [33]. The low heat capacity is a drawback of the paraffinic materials.

Thermal conductivity and effusivity data are listed in Table 4. Despite low thermal conductivity values of the three PCMs under discussion, the ECP conductivity is twice as a polyethylene glycol 1500-epoxy composite also designed for the latent heat energy storage [22, 33], e.g., 0.46 W m^{-1} K^{-1}. However, adding metallic fillers will improve these parameters. The effusivity values decreased in the same succession as the corresponding thermal conductivity (Eq. 1).

The density measurements were correlated with the decomposed DSC curves in order to establish the temperatures where the material is solid or liquid. Slight decrease in density of the crystalline form (ordered form) was recoded when increases the temperature (Fig. 8) up to initiation of the order–disorder transition (Table 5). At that temperature, density has a steep decrease. A slight increase of melt density was recorded in all the paraffinic samples up to the T_{on} of crystallization. In the peak zone, there is a possibility to establish the density for each zone (amorphous and different crystals but there are necessary other data for the composition of samples). However, our density calculation is limited to the melts and semicrystalline solids (Table 5). Since the density of the solid paraffins is higher than the paraffinic melts, volume variation during melting process triggers formation of the voids with different size, shape, and distribution in the places where these paraffins act as PCMs [36]. The formed voids affect further the rate of the melting/cooling cycling and can cause collapsing of the enclosing building elements [36]. All the paraffinic materials considered here presents considerable volume change (>12.4 %) at the ordered solid to melt transition. Hence micro- and/or maro-encapsulation of these paraffinic materials and shape [37] (cylindrical, spherical, and planar) and dimension of the building elements using these materials should be thoroughly considered.

Conclusions

Three phase change materials (PCMs), two commercial paraffins, E53 and E46, and a parafinic composite with ceresin, ECP, were thermophysically investigated in order to be implemented them in a pilot plant developed in Plovdiv. Raman investigation of the three materials revealed structural resemblance of the E46 and ECP samples due to their unsaturated content (compounds containing C=C bonds), higher in the latter case. Slight unsaturated character of the E46 and ECP materials might point out their liability to oxidation decreased thermal stability against long cycling use. The paraffinic content of the three PCMs and their latent heat decrease in the same succession, namely 194.32 J g^{-1} (E53), 176.77 J g^{-1} (E46) and 143.89 J g^{-1} (ECP). Moreover, the E53 paraffin encountered a two-phase transition, the lower temperature transition corresponds to the order–disorder transition and the second one to the melting of the disordered solid, while the E46 and ECP samples show a single very asymmetric peak of transition. Hence a three-peak model of the DSC curves was forwarded in order to describe the phase transition of the E46 and ECP samples on heating and/or cooling. The two lower temperature components were assumed to originate from the order–disorder and melting of the paraffin and the third DSC peak to the melting of the ceresin counterpart. The solid order–disorder character of the lowest temperature phase transition in the DSC runs is also supported by the steep decrease of the density values. The ceresin component triggers an increase of the thermal conductivity, i.e., 0.46 W m^{-1} K^{-1} for the ECP, while the conductivity value for the E53 and E46 is 0.33 W m^{-1} K^{-1}.

Due to its high latent heat, the E53 paraffin is a good PCM for latent heat storage purposes whose thermal conductivity can be improved by metal filler additions. On the other hand, better thermal conductivity originating in its ceresin content, not very low latent heat, and low price made of ECP composite a material to take in consideration for the same purposes. All the thermal data collected for these three paraffinic materials are due to modeling of the heat transfer in various geometries as preliminary step in implementing them in passive and/or active heat storage systems in buildings.

Acknowledgements Partially support of the EU (ERDF) and Romanian Government that allowed for acquisition of the research infrastructure under POS-CCE O 2.2.1 project INFRANANOCHEM - Nr. 19/01.03.2009, and Bulgarian research project 102ni063-24/05.05.2010 of the Technical University of Sofia, is gratefully acknowledged. Results were presented in frame of COST Action TU0802 NeCoE-PCM.

References

1. Jeon J, Lee J-H, Seo J, Jeong S-G, Kim S. Application of PCM thermal energy storage system to reduce building energy consumption. J Therm Anal Calorim. 2013;111:279–88.

2. Farid MM, Khudhair AM, Razack SAK, Al-Hallaj S. A review on phase change energy storage: materials and applications. Energy Convers Manag. 2004;45(9–10):1597–615.
3. Jeon J, Jeong SG, Lee JH, Seo J, Kim S. High thermal performance composite PCMs loading xGnP for application to building using radiant floor heating system. Sol Energy Mat Sol C. 2012;101:51–6.
4. Soares N, Costa JJ, Gaspar AR, Santos P. Review of passive PCM latent heat thermal energy storage systems towards buildings' energy efficiency. Energy Build. 2013;59:82–103.
5. Shukla A, Buddhi D, Sawhney RL. Thermal cycling test of few selected inorganic and organic phase change materials. Renew Energy. 2008;33(12):2606–14.
6. Zhang P, Song Y, Hu L, Lu HD, Wang J, Liu QQ. Synergistic effect of iron and intumescent flame retardant on shape-stabilized phase change material. Thermochim Acta. 2009;487:74–9.
7. Xu B, Li Z. Paraffin/diatomite composite phase change material incorporated cement-based composite for thermal energy storage. Appl Energy. 2013;105:229–37.
8. Xiao X, Zhang P, Li M. Preparation and thermal characterization of paraffin/metal foam composite phase change material. Appl Energy. 2013;112:1357–66.
9. Aydın AA, Okutan H. High-chain fatty acid esters of myristyl alcohol with even carbon number: novel organic phase change materials for thermal energy storage –1. Sol Energy Mat Sol C. 2011;95(8):2752–62.
10. Zhu JQ, Bai LG, Chen BH, Fei WY. Thermodynamical properties of phase change materials based on ionic liquids. Chem Eng J. 2009;147:58–62.
11. Cabeza LF. Materials used as PCM in thermal energy storage in buildings: a review. Renew Sustain Energy Rev. 2011;15(3):1675–95.
12. Py X, Olivès R, Mauran S. Paraffin/porous-graphite-matrix composite as a high and constant power thermal storage material. Int J Heat Mass Tran. 2001;44:2727–37.
13. Wu SY, Wang H, Xiao S, Zhu DH. An investigation of melting/freezing characteristics of nanoparticle-enhanced phase change materials. J Therm Anal Calorim. 2012;110:1127–31.
14. Ungar G, Zeng X-b. Learning polymer crystallization. Chem Rev. 2001;101(12):4157–88.
15. Sullivan PK. Solid-phase behavior of several long-chain *n*-paraffins, esters, and a ketone. J Res NBS A Phys Ch. 1974;78A(2):129–41.
16. Tyagi VV, Buddhi D. PCM thermal storage in buildings: a state of art. Renew Sustain Energy Rev. 2007;11(6):1146–66.
17. Fernandez AI, Sole A, Barreneche C, Martinez M, Martonell I, Miro L, Hadjeva M, Boudenne A, Bey Sana S, Magali F, Constantinescu M, Anghel EM, Malikova M, Krupa I, Penelosa C, Delgado M, Lazaro A, Paksoy HO, Yilmaz B, Bajare D, Sumiga B, Boh B, Haussmann T, Stefan S, Weber R, Fumarski P, Jarowski M, Cabeza LF. Characterization of PCM conventional and non-conventional technologies, Proceedings of the 2nd International Energy Storage Conference, Trinity College Dublin. 19–21 June 2013. pp. 85–91.
18. Giavarini C, Pochetti F. Characterization of petroleum products by DSC analysis. J Therm Analysis. 1973;5:83–94.
19. Mehling H, Cabeza LF. Heat and cold storage with PCM. Heat and Mass Transfer. Berlin Heidelberg: Springer Verlag; 2008.
20. Popov R, Georgiev A, SCADA system for study of the installation with solar collectors, charging phase change materials and borehole storage, Proceedings of the 2th International Energy Storage Conference, Trinity College Dublin. 19–21 June 2013. pp. 206–212.
21. Georgiev A, Tabakova S, Popov R, Valkov I, Moev S, Barzilova S, Lishev S, Takev M, Vassilev A, Boichev A. Construction and modeling of heat energy storage with phase change materials. J Technic Univ Sofia, branch Plovdiv. 2011;16(2):45–51.
22. Constantinescu M, Dumitrache L, Constantinescu D, Anghel EM, Popa VT, Stoica A, Olteanu M. Latent heat nano composite building materials. Eur Polym J. 2010;6:2247–54.
23. Kissinger HE. Variation of peak temperature with heating rate in differential thermal analysis. J Res Nat Bur Stan. 1956;57:217–21.
24. Wagner W, Kleinrahm R, Losch HW, Watson JTR. Hydrostatic Balance Densimeter with Magnetic Suspension. In: Goodwin A, Marsh KN, editors. Measurement of the "Measurement of the Thermodynamic Properties of Single Phases", Elsevier, 2003. Amsterdam: Elsevier; 2003. p. 125–219.
25. Edwards HGM, Falk MJP. Fourier-transform Raman spectroscopic study of unsaturated and saturated waxes. Spectrochim Acta, Part A. 1997;53(14):2685–94.
26. Zheng M, Du W. Phase behavior, conformations, thermodynamic properties, and molecular motion of multicomponent paraffin waxes: a Raman spectroscopy study. Vib Spectrosc. 2006;40:219–24.
27. Jehlicka J, Edwards HGM, Jorge Villar SE. Raman spectroscopy of natural accumulated paraffins from rocks: evenkite, ozokerite and hatchetine. Spectrochim Acta, Part A. 2007;68:1143–8.
28. Boerio FJ, Koening JL. Raman scattering in crystalline polyethylene. J Chem Phys. 1970;52:3425–31.
29. Dirand M, Bouroukba M, Chevallier V, Petitjean D, Behar E, Ruffier-Meray V. Normal alkanes, multialkane synthetic model mixtures, and real petroleum waxes: crystallographic structures, thermodynamic properties and crystallization. J Chem Eng Data. 2002;47:115–43.
30. Abbate S, Wunder SL, Zerbi G. Conformational dependence of Fermi resonances in *n*-alkanes. Raman spectra of 1,1,1,4,4,4-hexadeuteriobutane. J Phys Chem. 1984;88(3):593–600.
31. Hacura A, Kaczorowska B. Raman microscopic characterization of phase separation in binary *n*-alkane mixtures. J Mol Struct. 2005;744–747:581–4.
32. Zuckerman JL, Pushaw RJ, Perry BT, Wyner DM. Fabric coating containing energy absorbing phase change material and method of manufacturing same. US Pat. 2003;6660667:B2.
33. Pavel PM, Constantinescu M, Anghel EM, Olteanu M. Solidification of a PEG 1500-epoxy nanocomposite around a horizontal pipe. App Energy. 2012;89:482–9.
34. Hadjieva M, Kanev St, Argirov J. Thermophysical properties of some paraffins applicable to thermal energy storage. Sol Energy Mat Sol C. 1992;27(2):181–7.
35. Vyazovkin S, Burnham AK, Criado JM, Perez-Maqueda LA, Popescu C, Sbirrazzuoli N. ICTAC Kinetics Committee recommendations for performing kinetic computations on thermal data. Termochim Acta. 2011;520:1–19.
36. Assis E, Ziskind G, Letan R. Numerical and experimental study of solidification in a spherical shell. J Heat Trans-T ASME. 2009;131:024502-1-5.
37. Tyagi VV, Pandey AK, Kaushik C, Tyagi SK. Thermal performance evaluation of a solar air heater with and without thermal energy storage. J Therm Anal Calorim. 2012;107:1345–52.